

# Fast Algorithm for List Mode Back-Projection of Compton Scatter Camera Data<sup>1</sup>

Scott J. Wilderman<sup>1</sup>, W. Les Rogers<sup>2</sup>, Glenn F. Knoll<sup>1</sup> and John C. Engdahl<sup>3</sup>

<sup>1</sup>Department of Nuclear Engineering and Radiologic Sciences, University of Michigan

<sup>1</sup>Division of Nuclear Medicine, University of Michigan

<sup>3</sup>Applied Nuclear Imaging, Inc.

## Abstract

A fast algorithm is presented for back-projection of Compton camera projection data in a list mode fashion, in which the number of operations per photon per image slice scales at less than the dimension  $N$  of the reconstructed image. The method focuses on the mesh of grid lines which delineate the pixels in the image, rather than on the pixels themselves, and involves computation of the intersection of back-projected Compton cones with just the outermost edges in the image and those grid lines near these image boundary intersection points, for each plane (or slice) of the image. Depending on the orientation of the back projected cone and the image space grid lines, between 4 and  $N + 4$  determinations (by quadratic solution) of cone/mesh intersections are required per image slice per photon. Thus the total number of floating point operations per image slice scales as 4 to  $N + 4$  times the number of detected photons. Three dimensional back-projections can be obtained simply by stepping through the sequence of planes in the image space parallel to the Compton aperture. Back-projected images are presented, using data generated by Monte Carlo simulations of a practical detector configuration and various source distributions.

## I. INTRODUCTION

Researchers have been attempting to develop electronically collimated (Compton scatter) nuclear medicine imaging devices since the pioneering work of Singh and co-workers in the early 1980's [1]. The primary motivation for these efforts is the promise of very large gains in sensitivity for equivalent signal noise compared to mechanical collimators. For representative Compton and mechanically collimated systems, Clinthorne [2] and LeBlanc [3] have estimated quadruple sensitivity gains for imaging of technetium (isotope  $^{99m}\text{Tc}$ , gamma energy of 140.5 keV) at identical system  $FWHM$  of 7.8 mm, and twenty-fold increase for imaging iodine ( $^{131}\text{I}$ , gamma energy 364.4 keV), with improved resolution using the Compton aperture.

Reconstruction of images from Compton aperture projection data, however, is a computationally challenging task. To date, no exact analytical solutions applicable to a practical imaging device have been found, though Basko and co-workers have developed analytical solutions for several special cases. They have examined one dimensional cameras (in which the detector pairs are one dimensional parallel strips) [5], [6], and double scattering cameras (which requires that all detected events Compton scatter in two separate detectors prior

to absorption) [7], and they have presented (though not yet published) a method using an expansion in spherical harmonics to approximate the conic Compton projection data [8]. Planar projection data can be determined from the expansions, and a filtered back-projection applied to reconstruct the image.

Traditional iterative reconstruction techniques, have not proven tractable either, primarily because of the enormous size of the matrix required to describe the imaging system. For a viable Compton system, consisting of a 81 cm square scatter detector (with 1.2 mm spatial resolution and with energy recorded in 100 eV bins), and a cylindrical capture detector 25 cm in radius and 10 cm long (spatial resolution of 3 mm) [3] the number of elements of the system matrix  $M$  is roughly  $2.3 \times 10^{10}$  per voxel of the image. For an  $N$  dimensional image, direct reconstruction in  $2D$  would involve inversion of  $MN^2$  dimensional matrices, and iterative methods would require  $\sim 10^{14}$  recursive multiplications. In either case, thousands of terabytes of memory would be needed. Uritani [4] has proposed using a parallel plate collimator to limit the size of the system matrix by restricting the number of possible detector and energy deposition bins associated with each source voxel. However, the large loss in sensitivity due to the collimator (for Uritani, from 80 to 90%) completely negates the advantage of electronic collimation.

Since, in the general case, the number of detected events  $N_\gamma$  will be much smaller than the number of elements  $M$  in the full projection data set, list-mode reconstruction methods present themselves as possible alternatives to direct solution algorithms [10]. In such methods, each event is treated as a point in a continuous measurement space, rather than as contributing a count to a position and energy bin. Since the total number of counts will in general be three or four orders of magnitude smaller than the number of bins, the size of the matrices and number of operations required in solving the problem will be reduced by a like amount. In addition, this technique has the advantage of preserving accuracy of measurement data that would otherwise be lost in discretizing of energy and position. List-mode methods could be used either as part of a back-projection reconstruction algorithm, or as part of an iterative estimation-maximization algorithm (which may require a back-projection for either determination of weights or as a initial value for a solution).

The computational speed of a back-projection algorithm will be driven by the number of operations required to determine which of the source voxels are intersected by the back-projected cones for each of the detected gamma ray, given the positions and energy transfers of the interactions. Rohe and co-workers [9] have proposed two list-mode back-projection

<sup>1</sup>This work has been partially supported through Contract NCI 2RAO1 CA-32846-24.

algorithms. In the first, which they refer to as the "Source Space Tree Algorithm," the source space is broken into successive octants until the pixel level is reached. At each step, the distance of closest approach of the cone and the center of each octant is calculated to gauge whether the cone intersects the given octant, then sub-octant, or individual pixel. The number of searches that must be done then is more than the total number of voxels intersected, because of the overhead spent in elimination of non-intersected voxels. As a typical cone will intersect slightly more than  $N$  pixels in each of the  $N$  slices of the image, so the number of distance of approach computations for a three dimensional reconstruction must be greater than  $N_\gamma N^2$ , because of the overhead in the search. Additionally, because of the uncertainties involved in determining voxel intersection from just the distance of closest approach of the cone to the voxel center, this method will determine either too many or too few voxel intersections by 15-20/method proposed by Rohe works in a coordinate system with  $z$  along the cone axis, assumes a spherical image volume, and examines cone and voxel intersections at various distances along the cone axis. The smallest value of  $z$  for which the cone intersects the cylinder is first determined and an image space perpendicular to this position is imposed. Steps are taken radially along the arc of the cone, beginning with an angle determined by the source space center and the first interaction position, and axially out the cone axis. When pixels in this coordinate system are determined to be intersected, intersection variables must be converted to the source space coordinate system before they can be scored. This method has a slight advantage in that sometimes multiple pixels in a row or column of the cone-axis coordinate system can sometimes be scored in one step, but it has a large overhead because of the system transformations, and it underscores the number of intersected voxels by more than 10% unless the axial steps are less than 15% of the pixel dimension [9]. This last constraint results in significantly more than 1 computation per intersected voxel being required.

We present below an exact algorithm for the back-projection operation, which requires at most  $N_\gamma N^2$  distance calculations and as few as  $4N_\gamma N$  for 3D reconstruction.

## II. METHODS

The details of the method are presented here for the two dimensional case. Application to three dimensions is a simple matter of employing the 2D algorithm at each plane of the image.

Figure 1 is a schematic of a standard Compton camera interaction, with a typical back-projected cone sketched in. The well-known methodology for generating the equations of cones of possible source positions is very briefly summarized here. Since the position of both the initial Compton scatter (position  $(x_1, y_1, z_1)$  of the figure) and the final photo-absorption  $((x_2, y_2, z_2))$  have been measured, the direction of the gamma after the scatter, which is the cone axis for the back-projection, can easily be determined. The cone angle  $\gamma$  is of course the Compton scattering angle, and can nominally be determined

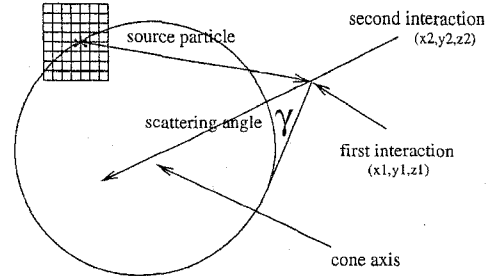


Fig. 1 Standard Compton camera back-projection.

Table 1  
Ellipse and mesh boundary intersection scenarios

1. does not intersect any edge
2. intersects an edge once but the opposite edge not at all.
3. intersects an edge once and the opposite edge once.
4. intersects an edge once and the opposite edge twice.
5. intersects an edge twice but the opposite not at all.
6. intersects two opposite edges twice each.

from the kinematic equations describing the scattering of a gamma ray from a free-electron at rest.

In the current algorithm, the source or image space is thought of as being divided not into solid voxels, but rather a series of planes (focal planes), each of which is divided by a series of mesh or grid lines which determine the pixels in that plane. For each detected event, then, a back-projected cone can be traced through to a given focal plane, which it will intersect in a manner as shown in figure 1. The quadratic describing the intersection of the cone with the plane (assumed to be located at  $z = z_s$ ) is given by

$$[n_x(x - x_1) + n_y(y - y_1) + n_z(z_s - z_1)]^2 = \lambda^2 [(x - x_1)^2 + (y - y_1)^2 + (z_s - z_1)^2], \quad (1)$$

where the  $n$ 's are the components of a unit vector along the cone axis and  $\lambda = \cos \gamma$ . The algorithm keys off how the conic (an ellipse) intersects the boundaries of the mesh in the image plane. There must be either 0, 2, 4, 6 or 8 intersections, which trace in the mesh either a full ellipse or 1, 2, 3, or 4 arcs, respectively, depending on the cone angle and cone axis. Disregarding non-unique cases due to symmetry in  $x$  and  $y$ , there are 11 types of possible edge intersection scenarios, which have been grouped into six cases for this analysis, as given in table 1. Several examples of the possible types of intersections are shown in figure 2. The amount of curvature in the inscribed arc will be determined primarily by the scattering angle, and, as for most Compton systems the arcs will not close within the image space, cases two and three will predominate, as indicated in figure 2.

The back-projection algorithm first solves equation 1, checking the four edges of the mesh in the given focal plane one by one for an intersection with the conic. Once an intersection

Table 2  
Marching algorithm rules for the six scenarios

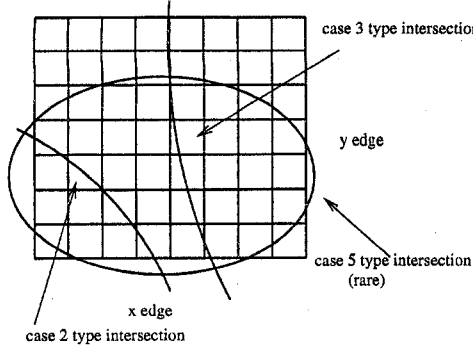


Fig. 2 Example of the edge/cone intersections

is found, it is checked to see whether or not it lies inside the image space, and the number of intersections of the ellipse with the opposite edge is then determined. Once the proper scenario of table 1 is identified, a marching algorithm is deployed subject to rules described in table 2 for the 6 scenarios.

In general, a march begins at a given mesh edge intersection and "steps" toward the opposite edge, looking for the intersection of the cone and the adjacent orthogonal grid lines. The coordinates of the nearest grid intersection determine how many pixel steps toward the opposite edge may be consumed in the step of the march pass. For example, if the march begins from an  $X$  edge at an  $x$  which lies between mesh lines at  $x = x_i$  and  $x = x_{i+1}$ , we look for intersections of the conic and these two grid lines. If there is no intercept at  $x_i$  and the intercept at  $x_{i+1}$  lies at  $y_j < y < y_{j+1}$ , we know that the cone intersects all image pixels  $I_{i,0}$  through  $I_{i,j}$ , and we can tally that many hits. An illustrative example is shown in figure 3.

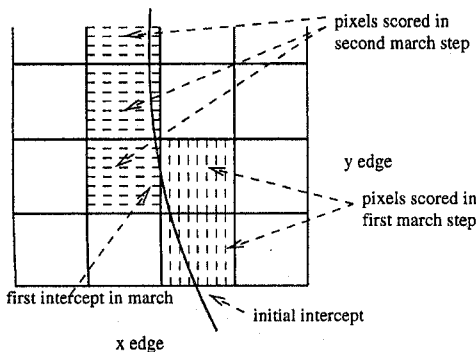


Fig. 3 Typical initial marching steps

For cones which are at higher angle and also aligned orthogonal to the grid (as they would be for a detector system using a parallel plate collimators [4]), no adjacent grid intersections will be present, and the marching algorithm can tally all pixels in the given row or column in a single step. In this case, just four quadratics would be solved, the two used to test the edges, and the two called to test the adjacent mesh lines. Tallies are performed along the lateral direction after each longitudinal step, until the image plane is completely

1. The ellipse is either wholly contained within the image boundaries or was generated by noise (e.g., multiple scattering in a single detector element) and should be rejected. Assess this by determining the intersection  $(x_c, y_c)$  of the axis with the image plane. If it's outside the image, reject. If not, find the intersection of the conic with the line  $x = x_c$  and start at that pixel, marching in both directions (left and right) to close the ellipse.
2. If the ellipse intersects just one of two opposite sets of edges, then it must intersect an edge orthogonal to the known edge of intersection. Start the march at the one known intersection point and proceed through the adjacent edge.
3. If opposite edges are intersected, the cone could inscribe an almost straight line (as in figure 2, or it could intersect one of the orthogonal edges twice. Start the march at one of the two known points. If an orthogonal edge is intersected (the latter case just described), do a second march from the second known intersection. If not, (the former case), quit.
4. In this case, the ellipse must intersect an adjacent edge. Do two marches, one from each point on the edge with two intersections, one of which will run through the orthogonal edge, and the other to the intersected adjacent edge.
5. Test both the orthogonal edges. If there are no intercepts, the cone curves inward at the intersected edge and then out again, so march from one known intercept to the other. Two orthogonal intercepts implies case three above, so march from each of the original intersection points. If there are four intercepts, switch to the orthogonal axes and apply case six below.
6. In this case, the ellipse could either close on itself outside each of the two opposite edges (similar to a pair of case three intersections) or it could intersect one or both orthogonal edges twice. In any event, do two marches from one of the known intersected edges. If an orthogonal edge is reached, another march must be done from the opposite edge.

swept. By proceeding in this way, the march remains one dimensional in each slice, meaning at most  $2N$  (in the case in which two diagonal marches must be made) steps are taken.

Each pixel which is determined to have been hit is scored  $1/n_h r_p$ , where  $n_h$  is the number of pixels hit, and  $r_p$  is the distance from the center of first detector element to the pixel center, to approximately account for the simple  $1/r$  dependence of the conic radius. Tallies for each photon are uniform, independent of the arc length of the ellipse inside the given pixel. An approximation in which the arc is treated as a straight line segment and the relative length of the segment in each pixel the tallying variable is currently being implemented.

The method is universally applicable to any Compton camera configuration, requiring only projection data in the form of lists of positions and energy losses of all coincident events in the given Compton camera imaging procedure.

### III. APPLICATION AND DISCUSSION

To test the method, projection data was generated by Monte Carlo simulation using the program SKEPTIC [11]. SKEPTIC

has been employed and tested extensively in numerous medical imaging applications [12], [13], including simulation of Compton scatter cameras [2], [3], [4], [14]. The program writes to disk lists of the exact interaction positions and energy losses, and the uncertainties in the measurements of these quantities are simulated by sampling from appropriate Gaussian distributions describing the energy and spatial resolution of the component detectors, as described in [14]. Doppler broadening of the scattered gamma spectrum, which has recently been found to be a limiting factor in the resolution performance of Compton cameras [15], is modeled using the tabulated data of Biggs [16] for amorphous silicon and of Reed [17] for crystalline silicon.

The detector system modeled is the C-SPRINT silicon and NaI system proposed by Clinthorne and LeBlanc [2],[3]. It consists of a 9x9 cm array of Si elements, divided into 1.2 mm cells. Each cell is 5 mm thick and assumed to have an energy resolution of roughly 250 eV, (an achievable level, as suggested by Weilhammer [18]). The capture detector is taken to be a hollow cylinder of NaI, 25 cm in radius and 10 cm long, with a spatial resolution of 3 mm.

Both  $^{99m}\text{Tc}$  and  $^{131}\text{I}$  sources were modeled. Spatial configurations of the sources included point sources in a cold background and hot rings of various radii and thicknesses in both cold and uniform warm backgrounds.

Figures 4 through 7 show reconstructed images for a  $^{99m}\text{Tc}$  point source located 10 cm from the front of the silicon detector, on-axis. The first image was produced using the exact position and energy data produced in the simulation (assuming perfect energy and spatial resolution), and, as all the back-projected cones pass through the source pixel, this image shows the roughly  $1/r$  blurring caused by the cones passing through neighboring elements in the image space. The second image was generated using the simulated measured data (the discrete first detector element positions, a sampled energy measurement, and a 3 mm *FWHM* second detector position), but without Doppler broadening. The third image, figure 6, was produced from the same data with Doppler broadening of the scattered photon energy also simulated, and the image of figure 7 that same image accounting for Doppler broadening in the case of crystalline silicon. The image space for all cases is a 64x64 pixels of 1 mm cells, and roughly 8,000 gamma rays were modeled. The effect of Doppler broadening is shown vividly by contrasting figures 5 and 6. The *FWHM* for the non-Doppler, Doppler, and crystalline Doppler cases shown are roughly 6, 12, and 14 mm, respectively, which, compares favorably with predictions [3].

A point source at  $^{131}\text{I}$  energy was also simulated and reconstructions performed. Images with and without the effects of Doppler broadening are presented in figures 8 and 9. As expected, as the Doppler broadening effect is fractionally less important for  $^{131}\text{I}$  than for  $^{99m}\text{Tc}$  because of the higher initial energy, sharper images are obtained.

Next, disks of outer radius 5 cm and inner radii of 4 and 1 cm were simulated, again for both  $^{131}\text{I}$  and  $^{99m}\text{Tc}$ . Reconstructed images for two of the cases are shown in figures 10 and 11. For the  $^{131}\text{I}$  image 35,000 photons were simulated,

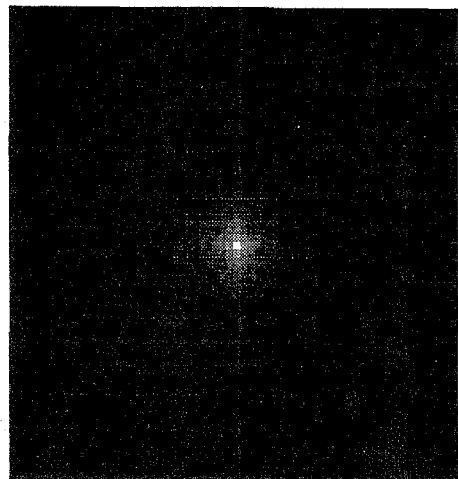


Fig. 4 Reconstructed Tc point source, exact positions

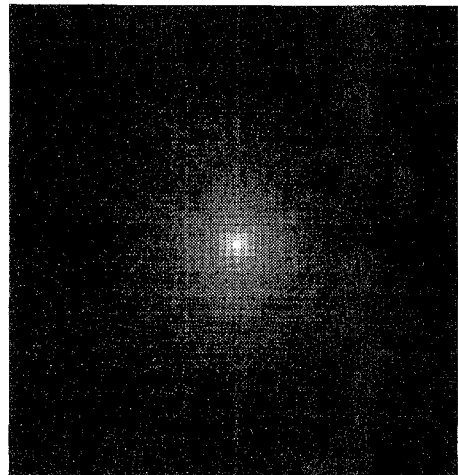


Fig. 5 Reconstructed Tc point source, measured parameters

and for the  $^{99m}\text{Tc}$  image, 150,000 photons. In both cases, the back-projections were done using assuming the image to be a 64x64 array of pixels 2 mm on a side, and Doppler broadening has been modeled. The central cold area in the thinner ring of the  $^{99m}\text{Tc}$  simulation is clearly visible, and the cold center of the thicker ring is discernible for the very small cold center simulated for  $^{131}\text{I}$ .

The average of the number of steps required for back-projecting an event for several of the cases above are shown in table 3. A histogram of the distribution of the number of steps for the  $^{99m}\text{Tc}$  ring case is shown in figure 12. Because of the azimuthal symmetry in the original Compton scatter, we expect symmetry in the distribution of back-projected cone orientations, and hence a fairly uniform distribution in the number of steps required for each photon. This is indeed seen in figure 12, and this results in a near constant value of  $4 + N/2$ , as expected, for the average number of steps, regardless of the spatial distribution of the sources, or the resolution of the

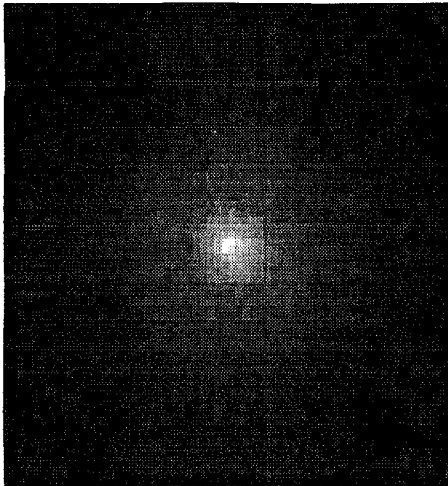


Fig. 6 Reconstructed Tc point source, with Doppler broadening

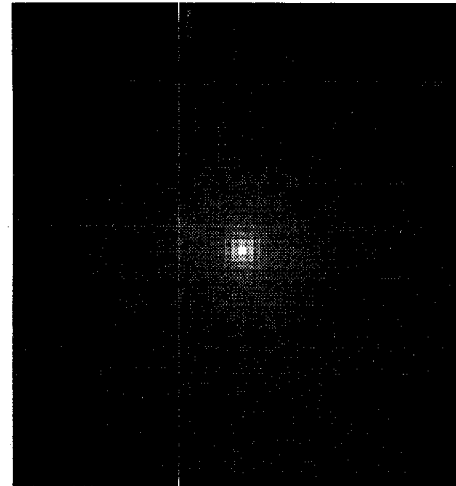


Fig. 8 Reconstructed  $^{131}\text{I}$  point source, without Doppler broadening

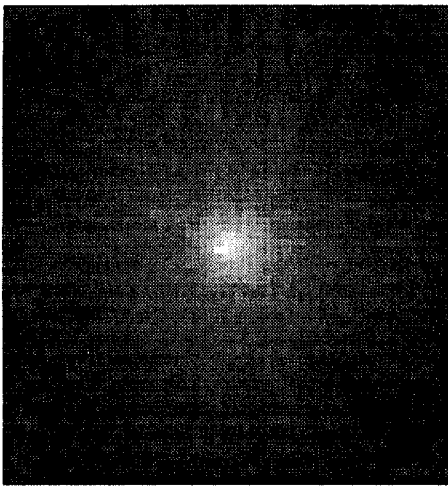


Fig. 7 Reconstructed Tc point source, Crystalline Si

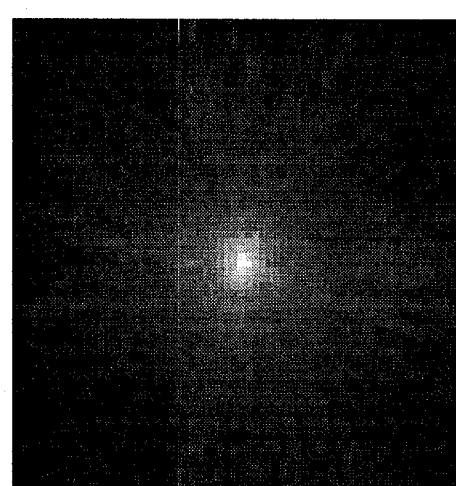


Fig. 9 Reconstructed  $^{131}\text{I}$  point source, with Doppler broadening

Table 3

Average number of back-projection steps per event

Reconstruction	Calls/event
$^{99m}\text{Tc}$ Point, Exact Positions, 32x32	19.33
$^{131}\text{I}$ Point, Doppler 64x64	37.47
$^{99m}\text{Tc}$ Ring Geometry 64x64	38.78
$^{131}\text{I}$ Ring Geometry 64x64	41.28

image, as seen in table 3.

#### IV. CONCLUSIONS

An exact, fast algorithm for back-projection of Compton camera data has been developed, and employed to reconstruct images from Monte Carlo simulated data. Images of 2D sources have been generated, and sources in input sources differentiated. The number of floating point operations required

for processing data sets representative of the size of those in nuclear medicine procedures has been determined to be reasonably small, especially in comparison with the number which would be required for direct reconstruction.

#### V. REFERENCES

- [1] M. Singh, "An electronically collimated gamma camera for single photon emission tomography. Part I: Theoretical considerations and design criteria," *Med. Phys.*, vol. 10, 1983 pp. 421-427.
- [2] N.H. Clinthorne, C-y Ng, C-h. Hua, J.E. Gormley, J.W. LeBlanc, D.K. Wehe, S.J. Wilderman, and W.L. Rogers, "Theoretical performance comparison of a Compton scatter aperture and parallel hole collimator," in Conference Record of the IEEE Nucl. Sci. Sym. *Anahiem, CA*, Nov 1996 pp. 788-792.
- [3] J.W. LeBlanc, N.H. Clinthorne, C-h. Hua, E. Nygard, W.L. Rogers, D.K. Wehe, P. Weilhamer, S.J. Wilderman,

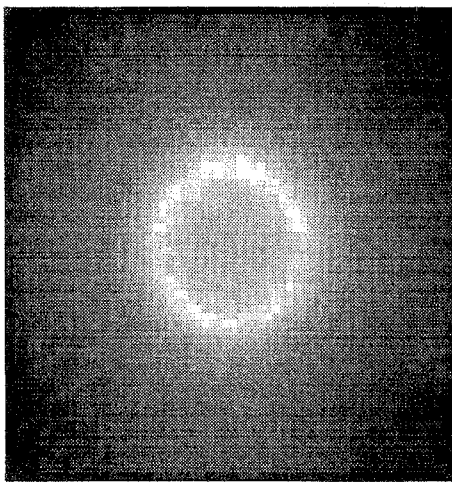


Fig. 10 Reconstructed  $^{99m}\text{Tc}$  disk source, cold spot of 4 cm

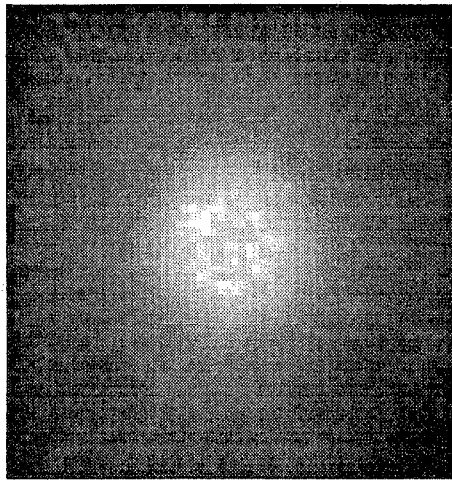


Fig. 11 Reconstructed  $^{131}\text{I}$  disk source, cold spot of 1 cm

- "C-Sprint: A prototype Compton camera system for low energy gamma ray imaging", presented at *IEEE Nucl. Sci. Sym. and Med. Imaging Conf., Albuquerque, N.M., 1997.*
- [4] A. Uritani, N.H. Clinthorne, J.E. Gormley, J.W. LeBlanc, W.L. Rogers, D.K. Wehe, and S.J. Wilderman, "An electronically collimated gamma camera with a parallel plate collimator for  $^{99m}\text{Tc}$  imaging," *IEEE Trans. Nucl. Sci., vol. 44, 1997 pp. 894-898.*
  - [5] R. Basko, G.L. Zeng, and G.T. Gullberg, "Analytical reconstruction formula for one-dimensional Compton Camera," *IEEE Trans. Nucl. Sci., vol. 44, 1997 pp. 1342-1346.*
  - [6] R. Basko, G.T. Gullberg and G.L. Zeng, "Using two one-dimensional Compton cameras of finite extent for transaxial tomography," *J. Nucl. Med., vol. 38, 1997 pp. 32-33.*
  - [7] R. Basko, G.L. Zeng, and G.T. Gullberg, "Fully three dimensional image reconstruction from 'V'-projections acquired by Compton camera with three vertex electronic collimation," presented at *IEEE Nucl. Sci. Sym. and Med. Imaging Conf., Albuquerque, N.M., 1997.*
  - [8] R. Basko, G.L. Zeng, and G.T. Gullberg, "Application of spherical harmonics to image reconstruction for Compton cameras," presented at *Int. Meeting on Fully 3-Dimensional Image Reconstruction in Radiology, 1997.*
  - [9] R.C. Rohe, M.M. Sharfi, K.A. Kecevar, J.D. Valentine, and C. Bonnerave, "The spatially-variant back-projection point kernel function of an energy-subtraction Compton scatter camera for medical imaging," in Conference Record of the IEEE Nucl. Sci. Sym. *Anahiem, CA, Nov 1996 pp. 1260-1264.*
  - [10] H.H. Barrett, T. White, and L.C. Parra, "List-mode likelihood," *J. Nucl. Med., vol. 37, 1996 pp. 124.*
  - [11] S.J. Wilderman, "Vectorized algorithms for the Monte Carlo simulation of kilovolt electron and photon transport," *University of Michigan, Ann Arbor, MI, Ph. D. dissertation, 1990.*
  - [12] M.J. Flynn, S.M. Hames, S.J. Wilderman, and J.J. Ciarelli, "Quantum noise in digital x-ray image detectors with optically coupled scintillators," *IEEE Trans. Nucl. Sci., vol. 43, 1996 pp. 2320-2325.*
  - [13] M.C. Wrobel, N.H. Clinthorne, J.A. Fessler, Y. Zhang, S.J. Wilderman, and W.L. Rogers, "Proposed method for correcting aperture penetration in high energy slit aperture and pinhole SPECT," *IEEE Trans. Nucl. Sci., vol. 44, 1997 pp. 1564-1570.*
  - [14] S.J. Wilderman, W.L. Rogers, G.F. Knoll and J.C. Engdahl, "Monte Carlo calculation of point spread functions of Compton scatter cameras," *IEEE Trans. Nucl. Sci., vol. 44, 1997 pp. 250-254.*
  - [15] C. Ordonez, A. Bolozdynya, and W. Chang, "Energy uncertainties in Compton scatter Cameras," presented at *IEEE Nucl. Sci. Sym. and Med. Imaging Conf., Albuquerque, N.M., 1997.*
  - [16] F. Biggs, L.B. Mendelsohn, and J.B. Mann, "Hartree-Fock Compton profiles for the elements," *At. Data Nuc. Data Tables, vol. 16, 1975 pp. 201-309.*
  - [17] W.A. Reed and P. Eisenberger, "Gamma-ray Compton profiles of diamond, silicon, and germanium," *Phys. Rev. B, vol. 6, 1972 pp. 4598-4604.*
  - [18] P. Weilhamer, *private communication, Nov 1996.*

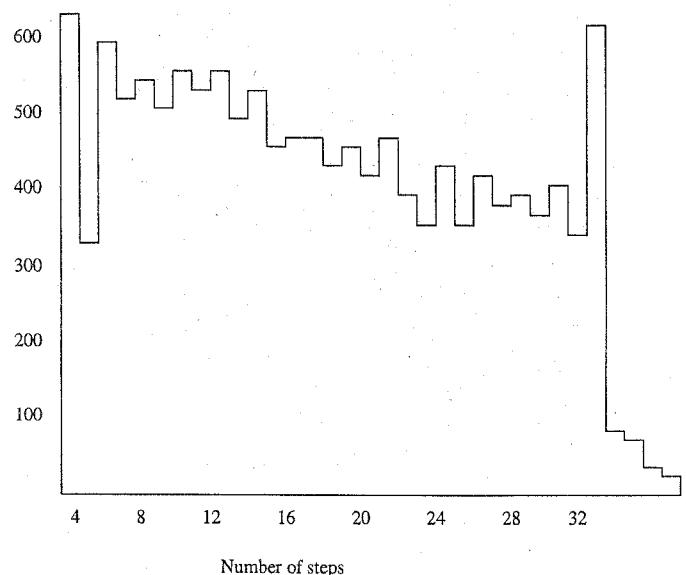


Fig. 12 Distribution of number of steps per photon

*Imaging Conf., Albuquerque, N.M., 1997.*